Airborne and UAV-borne Laser Bathymetry applied to a mountain river reach

Theresa Himmelsbach[1], Jan Rhomberg-Kauert[2], Gottfried Mandlburger[2], Wolfgang Dobler[1], Bernhard Gems[1], Markus Aufleger[1]

[1]Unit of Hydraulic Engineering, Faculty of Engineering Sciences, University Innsbruck, Austria – theresa.himmelsbach@uibk.ac.at
[2]Department of Geodesy and Geoinformation, TU Vienna, Austria – jan.rhomberg-kauert@geo.tuwien.ac.at

Keywords: Sensors, topo-bathymetric LiDAR, river morphology, rough riverbed, macro-roughness, flow resistance

Abstract

Mapping mountain river bathymetry poses significant challenges due to low flow depths, variable bed topography, and whitewater rapids, which hinder most survey techniques. This study explores the use of airborne and Unmanned Aerial Vehicle (UAV) laser bathymetry to address these challenges. Two topo-bathymetric *RIEGL* sensors, VQ-880-G (aircraft) and VQ-840-GL (UAV), were applied to a $500\,\mathrm{m}$ section of the Fischbach River in the Ötztaler Alps (Austria), characterized by step-pool morphology and high bed roughness. The surveys carried out under low flow conditions showed the superior performance of the VQ-840-GL in capturing detailed submerged topography due to its smaller footprint and closer point spacing. The VQ-880-G could capture broader features but lacked detail, in particular under water. Both systems failed to penetrate whitewater rapids. Despite these limitations, UAV-based laser bathymetry marks a significant step forward, enabling spatially continuous bathymetry data collection in complex mountain river settings, critical for advancing hydraulic and sediment transport research.

1. Introduction

Mapping the bathymetry of mountain rivers is much more challenging than that of gravel bed rivers. Their particular characteristics of a heterogeneous and highly structured riverbed with broad grain size distributions from gravel to large immobile boulders significantly influence flow conditions and thus bedload transport (Wohl, 2013). Mountain rivers pose a challenge to all survey techniques due to their highly variable riverbed topography (riffle-pool, step-pool, rough bed, etc.), shallow water depths, turbulent currents and whitewater rapids (Buffington and Montgomery, 2013). The lack of adequate survey techniques that can provide spatially continuous bathymetry data is a limiting factor in the progress of hydraulic and sediment transport research on mountain rivers with regard to the quantification of flow resistance (Ancey, 2020, Ferguson et al., 2024).

Spatially continuous submerged riverbed data are as essential for mountain river reaches as they are for gravel bed rivers. Surveying mountain rivers requires high point densities and small point-to-point spacing due to their complex morphology and high small-scale variability in bed topography with different grain sizes (Buffington and Montgomery, 2013). Unlike gravel bed rivers, where fewer data points may be sufficient to capture morphological variability, mountain rivers require higher spatial resolution than terrestrial surveying methods such as total stations or Global Navigation Satellite System (GNSS) can provide, given the river is wadable at all. Areas with significant bedform variation, such as step-pool systems, require narrower point spacing. While hydro-acoustic methods (e.g. single- or multi-beam sonar) are effective in increasing point density in deeper waters, they are generally unsuitable for mountain rivers due to minimum immersion depth and clearance from the bed (Lague and Feldmann, 2020). Stereo image analysis and Structure from Motion (SfM), derived from aerial photogrammetry with high-resolution, multispectral cameras, are sensitive to water clarity, bed visibility, and surface smoothness. Measurement depths of up to $1.5\,\mathrm{m}$ are only possible under optimal conditions, which are rarely encountered in turbulent mountain rivers (Legleiter et al., 2016). Light refraction at the water surface requires data correction (Dietrich, 2017). Infrared (IR) laser systems provide detailed 3D mapping of dry surfaces with high point density due to a small footprint diameter and high point accuracy (Stammberger et al., 2024). However, IR laser scanning is ineffective in penetrating water, as its signals are reflected or absorbed by the water surface, which is used to detect the water surface (Mandlburger et al., 2020b).

Laser bathymetry uses a green wavelength of the electromagnetic spectrum ($532\,\mathrm{nm}$), which penetrates the water column. The emitted laser pulse travels through the atmosphere to the water surface, where part of it is reflected (Mandlburger, 2022). The remaining laser energy travels through the water column at a reduced propagation speed until it reaches the bottom of the river and is backscattered to the receiver located on the operating platform. The water depth is derived from the time of flight between the transmitted laser signal and the backscattered water bottom echo, taking into account the refraction of light. Shallow water systems (topo-bathymetry), compared to deep water systems, are suitable for watercourses due to their short pulse duration, low energy, high repetition rate and small beam footprint diameter (Mandlburger, 2022). Georeferencing is achieved using GNSS and Inertial Measurement Systems (IMS) systems. The achievable penetration depth depends on both the sensor and environmental factors such as turbidity, vegetation, and air bubbles, which scatter and attenuate the beam, leading to premature reflections (Lague and Feldmann, 2020, Frizzle et al., 2024). Beam deflection and reduced propagation speed in water cause depth overestimation, requiring refraction corrections based on accurate 3D water surface models. In shallow water (<15 cm), water surface echo and water bottom echoes can overlap, making depth detection difficult (Lague and Feldmann, 2020). Modern systems address this by recording the entire backscatter signal, also referred to as full waveform data (FWF). To improve echo detection and point density, full waveform data can be processed on board through online waveform processing (OWP) or offline with special waveform algorithms (Schwarz et al., 2019, Mandlburger et al., 2023).

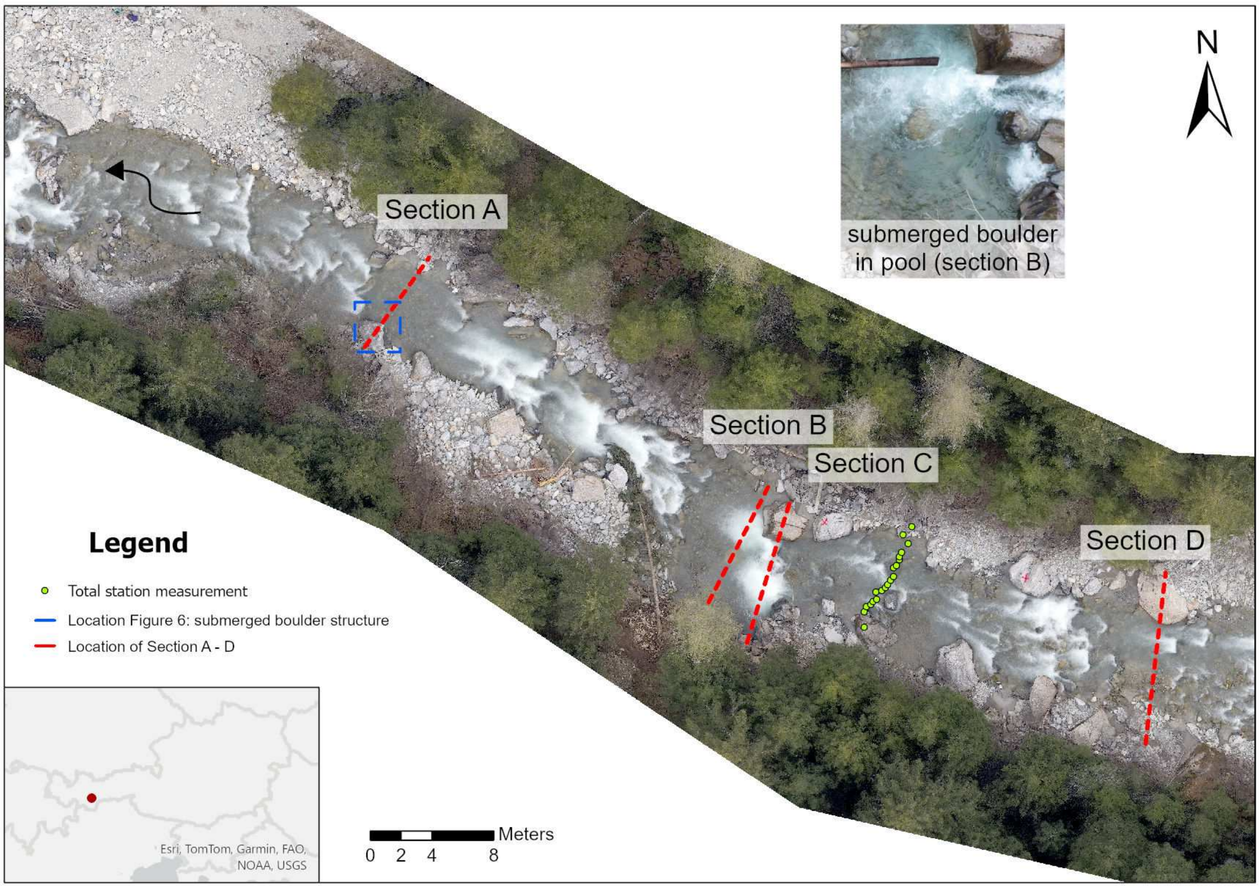

Figure 1. Section of the Fischbach River in Tyrol, Austria, with locations of evaluated Sections A – D.

The geometric variability of mountain riverbed topography requires small footprints and short point-to-point distances. Small footprints result from small laser beam divergence and low operating heights. High pulse repetition rates result in small point-to-point distances. Overlapping flight strips are generally used to increase the point density. The high variability in flow depth from deep pools to very shallow flows in mountain rivers requires a short pulse duration to discriminate between water surface and bottom echoes (Mandlburger et al., 2023). Whitewater rapids in step-pool systems are thought to behave like high turbidity, backscattering the echo from the surface and leaving no energy left to reach the river bottom (Lague and Feldmann, 2020).

The resulting point cloud is influenced by the height and operating speed of the sensor-carrying platform. While altitude influences the resulting footprint diameter and the point-to-point spacing, operating speed determines scan lines spacing. The introduction of miniaturized sensors with smaller dimensions and lower transport weight allows the use of Unmanned Aerial Vehicles (UAVs) as carrier platforms (Kinzel et al., 2021, Wang et al., 2022, Mandlburger et al., 2023). UAV-operated sensors allow lower operating altitudes and slower platform speeds, which together with the low beam divergence result in small footprints and high point density (Mandlburger et al., 2020a). With these features, UAV-based laser bathymetry provides the appropriate conditions to potentially address the challenges of capturing mountain river bathymetry (Wang et al., 2022).

The aim of this contribution is to investigate the capabilities of laser bathymetry on a mountain river reach, by comparing two different generations of sensors from the same manufacturer, operated from their typical carrying platforms.

The paper is structured as follows: Section 2 presents the surveyed mountain river reach, details of the data acquisition, and the evaluation methods. Section 3 examines the laser bathymetry data at morphologically interesting locations along the river reach. Section 4 discusses the findings, and Section 5 closes the contribution with concluding remarks and recommendations on future work.

2. Material and Methods

In this section, the study site is introduced (Section 2.1) and the data acquisition and evaluation methods are presented (Section 2.2).

2.1 Study site

The study site is a $500\,\mathrm{m}$ section of the Fischbach River, a mountain river in the Ötztal Alps, Tyrol, Austria (loc.: 47.073328 N, 11.004194 E). The study reach is located at an altitude of about $1500\,\mathrm{m}$ and is fed by the Sulztal glacier. The reach has a bed slope of approximately $8\,\%$ and is characterized by a rough bed and step-pool morphology, a broad grain size distribution with a $D_m = 110\,\mathrm{mm}$ and large immobile boulders ($> 265\,\mathrm{mm}$). Boulders are located along the sides of the main channel or form the steps of step-pool systems. Some isolated, fully submerged boulders are in the thalweg, such as in cross section B of the site (Figure 1). The Fischbach River has a nivo-glacial flow regime with an average annual discharge of about $3.5\,\mathrm{m}^3/\mathrm{s}$ and the lowest discharge in the winter month of about $0.5\,\mathrm{m}^3/\mathrm{s}$.

2.2 Methods

The Fischbach River was surveyed using two different laser bathymetry sensors, the VQ-880-G and VQ-840-GL sensors from *RIEGL*. The laser bathymetry surveys were conducted in February 2024 (VQ-880-G) and April 2024 (VQ-840-GL) under low flow conditions and clear water visibility. The discharge on the day of the surveys was $0.5\,\mathrm{m}^3/\mathrm{s}$ and $1.4\,\mathrm{m}^3/\mathrm{s}$, respectively. During the February survey, the river banks were covered with snow in some places, but the main channel was free of snow. During the April survey campaign, the river stretch was completely free of snow.

The VQ-880-G was operated from a fixed-wing aircraft at $400\,\mathrm{m}$ to $600\,\mathrm{m}$ above ground level (AGL) (using a descending and ascending flight pattern due to the narrow valley) at an operating speed of $120\,\mathrm{knots}$ ($61\,\mathrm{m/s}$). Turning and mountain flanks required a higher flight altitude. The sensor was operated at a pulse repetition rate (PRR) of $550\,\mathrm{kHz}$ and a beam divergence of $0.7\,\mathrm{mrad}$. The VQ-840-GL was operated from a UAV at $102\,\mathrm{m} \pm 14\,\mathrm{m}$ AGL with an operating speed of $5\,\mathrm{m/s}$. The VQ-840-GL sensor was operated at a pulse repetition rate of $200\,\mathrm{kHz}$ and a beam divergence of $2.0\,\mathrm{mrad}$. The resulting footprint diameter at the water surface was approximately $0.3\,\mathrm{m}$ to $0.4\,\mathrm{m}$ for the aircraft-operated VQ-880-G and approximately $0.2\,\mathrm{m}$ for the UAV-operated VQ-840-GL survey. From this point onward, data from the VQ-880-G aircraft-operated sensor will be referred to as 'ALB' (Airborne Laser Bathymetry) data, and data from the VQ-840-GL UAV-operated sensor will be referred to as 'ULB' (UAV-borne Laser Bathymetry) data.

Sensor	PRR [kHz]	Beam divergence [mrad]	Operating altitude [m AGL]	Platform speed [m/s]
VQ-880-G	550	0.7	400-600	61
VQ-840-GL	200	2.0	102	5

Table 1. Sensor details and platform operation parameters

The full waveform data from the ALB survey was post-processed, while the ULB data underwent online waveform processing (OWP) (Pfennigbauer et al., 2014). The ALB data were georeferenced using a $0.5\,\mathrm{m}$ gridded reference digital terrain model (DTM) provided by the federal state of Tyrol. Due to the shading effects of the steep valley, the GNSS georeference measurements for the ULB survey suffered from large deviations. Therefore, the ULB data was subsequently georeferenced using the Tyrolean DTM.

The refraction correction required by the penetrating laser beam entering the water column could only be performed for the ULB data. Due to the extremely low discharge during the ALB survey campaign, and the difficulty of distinguishing between the water surface and river bottom points, it was not possible to derive a water surface model and to carry out refraction correction.This means that the ALB's riverbed data points are expected to have lower z-elevations.

In addition, an aerial photogrammetry survey for the dry riverbed area was carried out during the survey campaign in April 2024. At the end of the year 2024, during the falling limb of the discharge curve at approximately $0.7\,\mathrm{m}^3/\mathrm{s}$, selected submerged areas were surveyed as cross sections using a total station (Figure 1, selected section).

To investigate the ability of the sensors to reproduce the submerged riverbed structure of mountain river reaches, we compared the two laser bathymetry datasets at selected locations following morphological units. We used only a single strip for each sensor to avoid misinterpretation of the resulting point densities due to overlapping flight strips. The strips have the same scanning direction. The selected sites are marked in Figure 1. For both strips, vegetation points, false echoes, and points identified as noise have been filtered out. The ULB dataset is fully classified with dry terrain points colored brown, water surface colored blue, river bottom colored dark grey, and very shallow submerged terrain, where water surface and river bottom echoes cannot be separated, in light grey. The ALB dataset is not further classified. ALB data points colored in red are either water surface or river bottom points.

Although the river reach was surveyed over a distance of $1.5\,\mathrm{km}$ with ALB and $0.5\,\mathrm{km}$ with ULB, only a $90\,\mathrm{m}$ long section was used for the study. This section was extracted using the same segmentation polygon. In order to capture the highly variable riverbed topography of mountain rivers, the ALB and ULB data are compared at various morphologically interesting locations. First, the data are compared at a shallow, clearly defined cross section location, without the influence of whitewater or protruding boulders, but with a large boulder on the river bank. This boulder enables us to compare georeferencing and the sensors' ability to reproduce topographic features without the influence of water. To investigate sensor capabilities in typical mountain river sections, we further selected a section with a large submerged boulder element, a whitewater section to compare penetration capabilities, and a very shallow site.

We also investigate the ability to reproduce submerged boulders at location A (Figure 1) and compare the cross sectional point density of the ALB with the point density of a total station survey. We compare the dataset using sections with approximately $0.5\,\mathrm{m}$ width in a cross section view, but also investigate point density and point spacing.

3. Results

A comparison of the airborne ALB dataset and the UAV-operated ULB dataset, both covering the same area, confirmed significant differences in the total number of points and total point density. Table 2 compares the number of points for the full section for each sensor, respectively, as well as for the filtered datasets. Filtered points are vegetation, false echoes, and noise. The water surface points are not filtered. The average point density was calculated based on a $1\,\mathrm{x}1\mathrm{m}^2$ raster cell. While the filtered, single strip of the ALB has an average point density of only about 9 points per square meter, the filtered, single strip of the ULB provides a point density of about 211 points per square meter. The vegetation on the riverbank is dominated by dense coniferous trees. Approximately 36,000 of the 54,985 points in the ALB data set were classified as vegetation.

Comparing the data sets, significant differences in the point-to-point spacing within and between the scan lines for the ALB and ULB data were apparent (Figures 2). For the ALB, the point-to-point distance within the scan line is approximately $0.26\,\mathrm{m}$. The ALB produced a regular scan pattern with, by visual judgment, regular distances between successive scan

https://doi.org/10.5194/isprs-archives-XLVIII-2-W10-2025-131-2025 | © Author(s) 2025. CC BY 4.0 License.

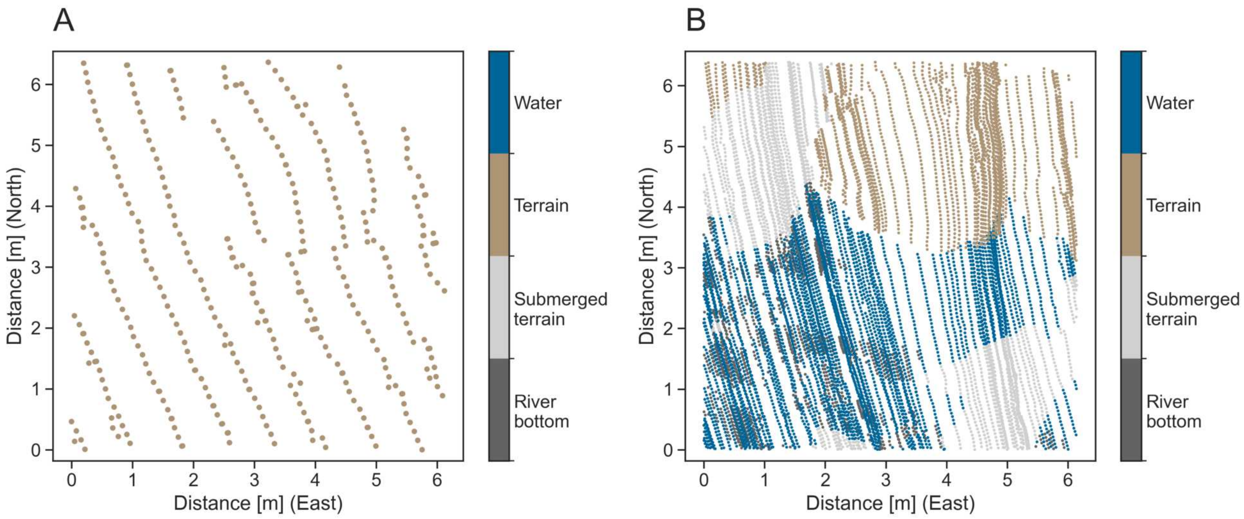

Figure 2. Detail of the ALB (left) and ULB (right) data at the same location with the same extent showing the different point-to-point distances within and between the scan lines.

Sensor	Total number of points		Point density [points/m^2]	
	full	filtered	full	filtered
VQ-880-G	54,985	13,110	30.3	8.8
VQ-840-GL	1,033,912	355,623	566.5	210.9

Table 2. Comparison of the total number of points and point density for the ALB data and the ULB data, for the full and the filtered strip respectively.

lines of approximately 0.7 m. For the ULB, the point-to-point distance within the scan line is approximately 0.07 m. Visually, the scan pattern of the ULB is affected by wind, with the distance between consecutive scan lines ranging from approximately 0.02 m to 0.45 m.

The ALB and ULB data are further analyzed by four different sections along the river reach. The location of each section is shown in Figure 1 and each individual section in Figure 4. Figure 4 are cross sectional visualizations of each section. The ULB data points have a smaller diameter and are colored in the colors blue for water surface, brown for terrain dry, light grey for shallow submerged terrain and dark grey for river bottom points. The ALB data points are larger in size and are all, water surface and river bottom points, colored in red.

Section A has a well-defined trapezoidal river cross section with a boulder element on each river bank and clear water conditions, as shown in Figure 1. In the ULB data, the water surface and the river bottom with a water depth of 0.28 m are identifiable, with data points spatially covering the entire river bottom (Figure 4a). The ALB data points also show a visible separation of the water surface and the river bottom points. The red ALB data points on the large boulder on the left have the same z-elevation as the ULB data, indicating a matching georeferencing. However, the channel data points are at lower elevation than the ULB data points. The water surface data points are lower due to the lower flow depth on the day of the survey, and the bottom points are lower due to a missing bottom point refraction (the true river bottom is approximately 0.25 % times higher than the raw river bottom). This demonstrates the overestimation of the river bottom depth and the importance of the refraction. Figure 3 shows

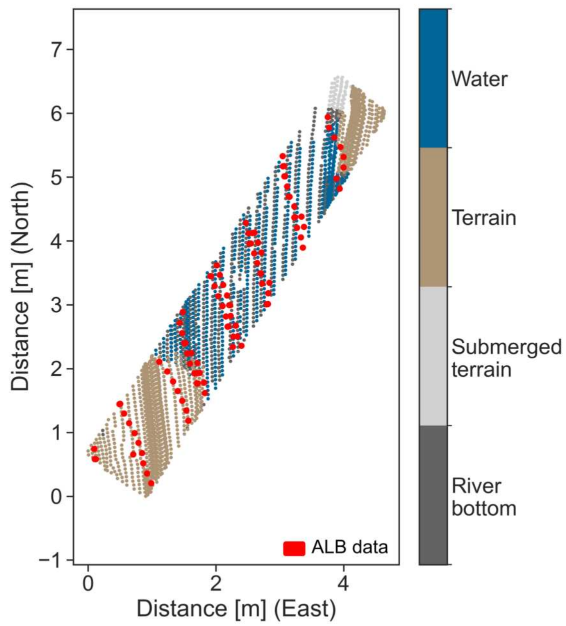

Figure 3. Planar view of section A with ALB data (large red dots) and ULB data points (small points, colored).

the water surface point and a corresponding river bottom point through two closely spaced points for both datasets, the ALB and ULB. It also shows the different resulting point densities for the ALB and ULB sensors for a 0.5 m strip width.

Figure 4 b shows the Section B with a submerged boulder element in the pool area. The submerged boulder element is visible in the ULB data, but not in the ALB data. If the continuous red ALB data points are assumed to be the water surface, then there are hardly any river bottom data points available in this section.

Section C (Figure 4 c) is a section of the large pool heavily influenced by whitewater with boulders on the river banks and an overflown boulder on the right of the channel (see Figure 1). In the ULB data, the bottom of the river is detectable only on the

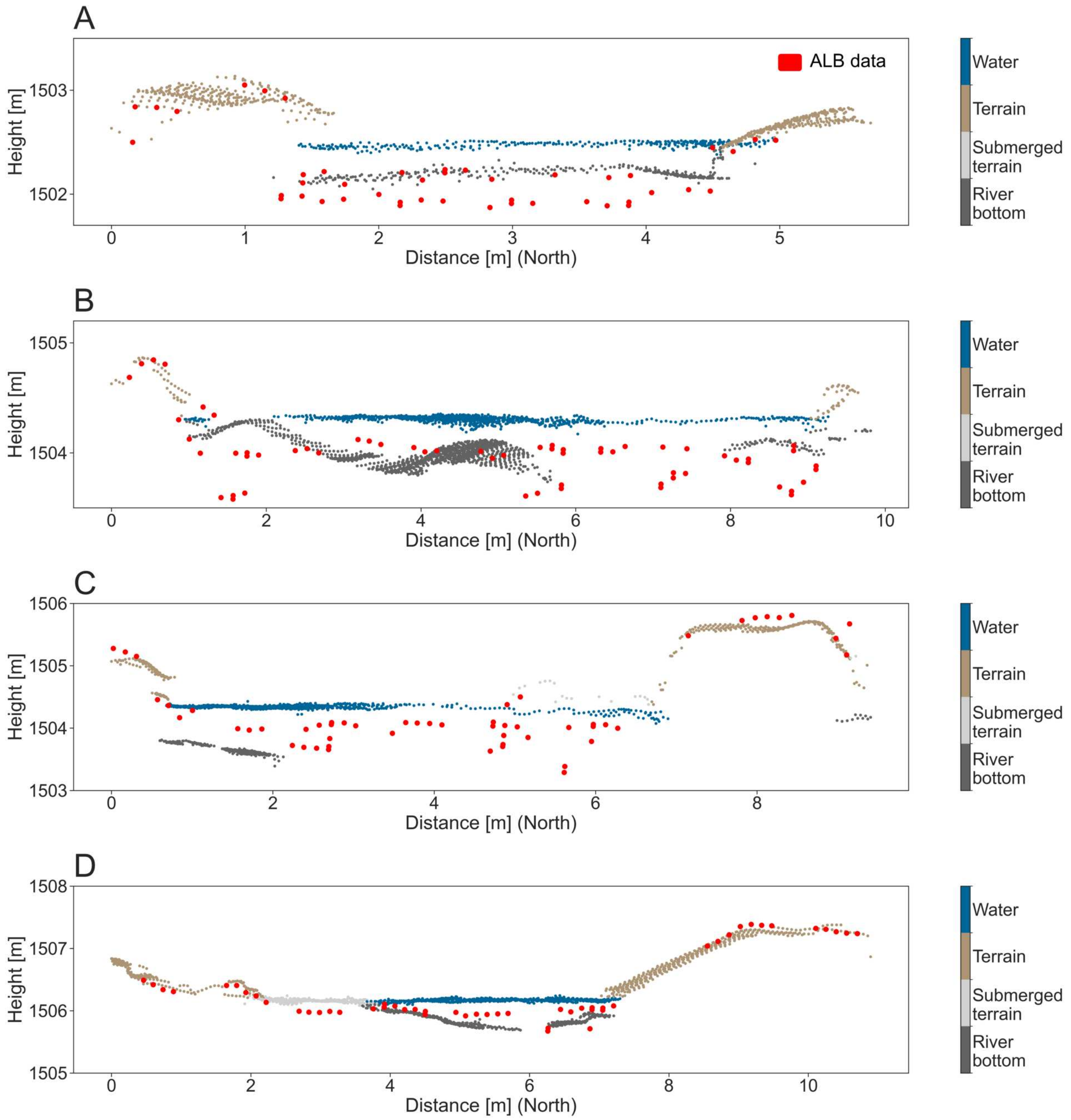

Figure 4. Cross sectional views in flow direction of the ALB data in red dots (water surface and river bottom points) compared to the classified data of the ULB (blue = water surface; brown = terrain dry, light grey = shallow submerged terrain; dark grey = river bottom).

side, but not below the main whitewater area. The ALB data is consistent with the river bank boulders, indicating the tendency of a water surface, but is diffuse below the water surface points in the whitewater area.

Section D in Figure 4 d is a heterogeneous section with some very shallow parts on the left and a slightly deeper part on the right. Again, the data points from both sensors agree in height and location for the dry part of the boulder element on the right riverbank. The points in the slightly deeper area on the right can be separated into the water surface and the bottom of the river for the ULB data. For the ALB data, the data points on the right could be identified as the water surface, with few isolated points from the riverbed.

Figure 5 shows a cross section view of the ALB data (red dots), the ULB data (small dots, colored according to classification) and the total station reference measurement (white squares). A comparison of the number of ALB data points and the total station data points manually surveyed along a $0.8\,\mathrm{m}$ wide cross section shows the number of points for each survey technique. The manually surveyed cross section data consists of 20 data points. The ALB data for the $0.8\,\mathrm{m}$ wide cross section contains approximately four times as many data points.

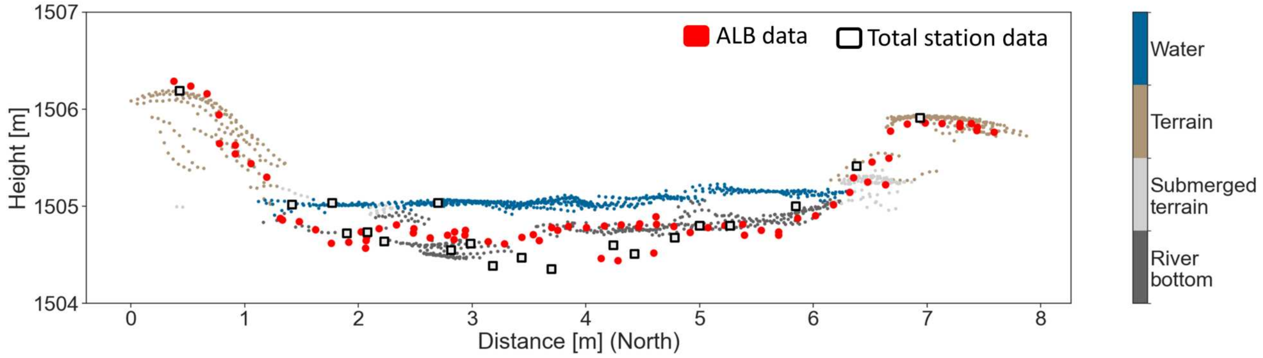

Figure 5. Comparison of the data point density along a cross section with a width of $0.8\,\mathrm{m}$. ALB data points in red, ULB data points small, in classification color, total station data points in white with black border (large).

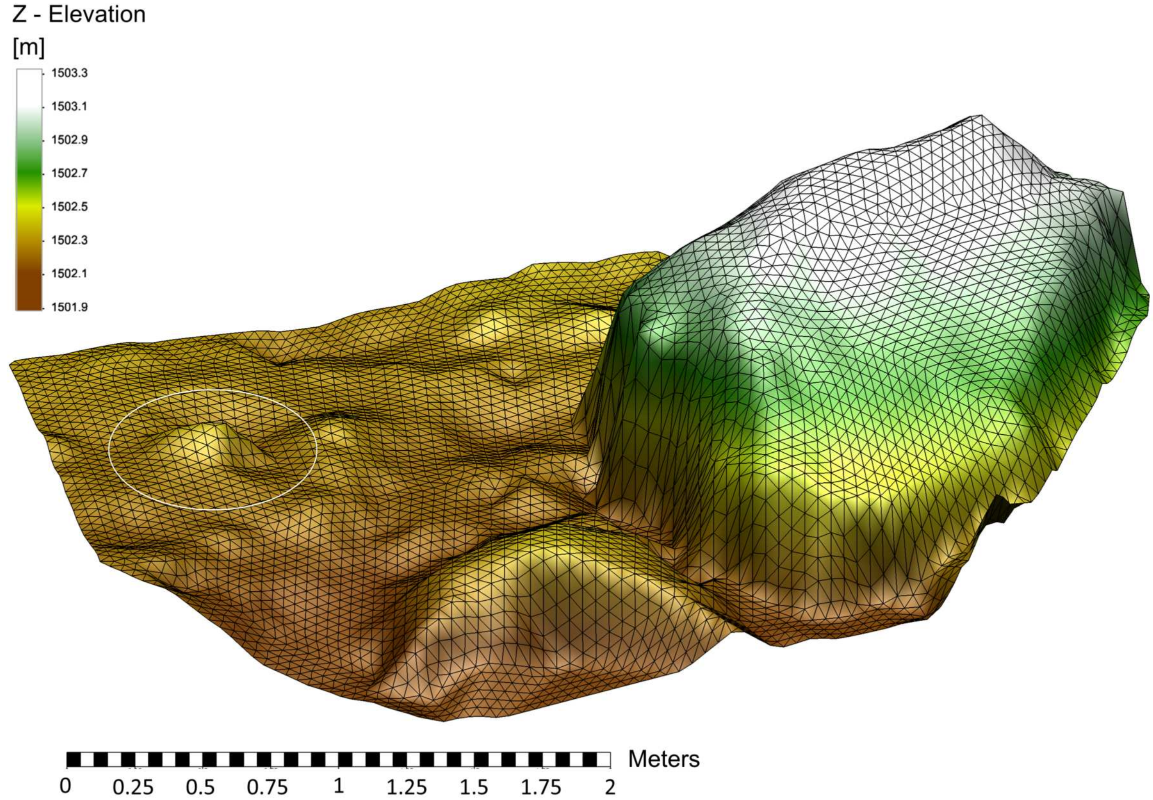

Figure 6. Submerged boulder element near Section A (circled, location see Figure 1) detectable in the ULB data and compared to a large boulder on the riverbank.

Figure 6 is a detail near Section A (Figure 1) and shows a submerged boulder element measuring approximately $0.3\,\mathrm{cm}$ on the left (circled), an overflowed boulder in the step and an large boulder measuring approximately $2\,\mathrm{m}$ on the riverbank. The generated mesh is based on data points from a single strip. The point density of the ULB data enables boulder elements to be detected and reconstructed at sub-meter resolution.

Although morphological riparian features above the water surface are clearly detectable in the ULB single strip, this is not the case for the ALB single strip due to the footprint size and the point-to-point distance within and between the scan lines. The point density of the ALB can to some extent reproduce boulders protruding above the water surface, however the river bed cannot be fully detected. In addition, the limited number of points impedes the separation between the water surface and the bottom echo. The roughness of the riverbed in very shallow flow sections is detectable as geometric variability in the data points for the ULB. However, neither data set was able to provide bathymetry points in strong whitewater rapids.

4. Discussion

The research on mountain river reaches has been limited by the methods available to collect bathymetry data. The scarcity of points for total station or GNSS measurements, compounded by often difficult river access, high variability of riverbed structure within a cross section and dangerous rapids for the surveying personal, hinders necessary progress in understanding and predicting hydraulic and bedload transport processes in mountain river reaches (Ancey, 2020, Ferguson et al., 2024).

Comparison of laser bathymetry data from an aircraft-operated *RIEGL* VQ-880-G sensor with data from a UAV-operated miniaturized *RIEGL* VQ-840-GL sensor revealed superior performance of the latter in capturing detailed submerged topography due to its smaller footprint and closer point-to-point spacing. While the VQ-880-G could only provide a point-to-point spacing slightly above that of a total station measurement within a cross-section, the UAV-operated VQ-840-GL was capable of reproducing submerged boulder elements using a single strip of data points. Both systems were unable to penetrate the whitewater rapids.

Although the VQ-880-G was operated with sensor settings that were better suited to small footprints and high point densities, it was not able to reproduce the structure of the riverbed equally well as the VQ-840-GL. This demonstrates the influence of operating height and platform speed. The VQ-880-G was operated with a beam divergence of 0.7 mrad, resulting in a footprint diameter of approximately $0.4\,\mathrm{m}$ at an operating altitude of $400\,\mathrm{m}$ to $600\,\mathrm{m}$ AGL, and a high pulse repetition rate of $550\,\mathrm{kHz}$. The VQ-840-GL sensor, operated at a lower pulse repetition rate of $200\,\mathrm{kHz}$ and a higher beam divergence of $2.0\,\mathrm{mrad}$ (resulting in a footprint diameter of approximately $0.2\,\mathrm{m}$), provided an average point density of 211 points per square meter for a single strip and was able to detect underwater boulder elements. Not only the sensor settings, but especially the carrier platform and the operation of the sensor, including operating height and platform speed, are essential factors in object detection. Overlapping flight strips would increase for both datasets the overall point density. However, it must be taken into account that the accuracy of object detection is determined by the diameter of the footprint. Although aircraft-operated sensors allow for efficient capture of longer river reaches, UAV-operated miniaturized sensors are more suitable for surveying small-scale heterogeneous rough riverbeds (Wang et al., 2022).

Challenges for laser bathymetry on mountain river reaches remain due their specific characteristics. The locally very shallow flow depth over rough riverbed sections or step overflows may not allow signal separation between the water surface and the river bottom echoes, neither with the help of full waveform post-processing (Frizzle et al., 2024). Very shallow flow depths during low discharge seasons and turbulent water surfaces can cause difficulties in refraction correction, resulting in incorrect river bottom elevations. To date, whitewater rapids do not allow riverbed detection in step-pool sections. And point cloud classification of complex morphologies with high point densities, submerged or dry, is very time- and labor intensive (Lague and Feldmann, 2020).

Mountain rivers such as the Fischbach River, located on altitudes above $1000\,\mathrm{m}$ have short time windows for survey campaigns. Although total station reference measurements are only possible during wadable, very low discharge periods with low flow velocities in the winter months, snow cover on the banks and on protruding boulders hinders laser bathymetry measurements. In addition, the shallow flow depth makes it difficult to separate the water surface and river bottom signals and to refract the data. Mountain rivers with nivo-glacial flow regimes, where discharge is highest during the summer months, have a high turbidity due to glacier melt. Snow-melt temperatures in the valley simultaneously initiate the melting process in glacier-covered catchments. As temperatures fall in the autumn, reducing glacier-fed discharge from the catchment, the snow line can drop rapidly, making it impossible to conduct survey campaigns. As a result, the window of opportunity for laser bathymetry surveys of mountain stream reaches is very limited to a few weeks in spring and fall each year.

5. Conclusion

The ability to survey mountain river reaches with more than just a total station opens up new opportunities for hydraulic and sediment transport research on rough river beds. In this study the *RIEGL* VQ-880-G and VQ-840-GL sensors were used on a mountain river reach. Future studies could apply these sensors on other morphological interesting river reaches or could focus on testing other commercially available UAV-operated miniaturized sensors with similar beam divergence, pulse duration, and pulse repetition rate characteristics on mountain river reaches. Particular attention should be paid to the timing of the survey campaign to ensure that reference measurements are taken as simultaneously as possible, before increasing flows alter the submerged river topography. Further studies could focus on laser penetration in turbulent whitewater rapids and echo separation in very shallow flow depth sections with full waveform processing (Mandlburger et al., 2023). Overall, the miniaturization of laser bathymetry sensors is enabling a new field of application. These advances in the acquisition of continuous bathymetric data of mountain rivers at spatially comprehensive scales open up new possibilities for hydraulic research, e.g., the estimation of flow resistance based on topographic roughness (Ferguson et al., 2024).

6. Acknowledgments

The airborne and UAV-borne laser bathymetry data of the Fischbach mountain river is part of the project ‘Meeting challenges in bedload transport of mountain rivers with advances in remote sensing techniques’, which was funded by the Tyrolean Young Scientists research grant TNF 2023 (grant number F.47887/5-2023). The authors would like to acknowledge the support of AHM GmbH and Skyability GmbH for the data acquisition and preliminary processing, and would like to thank TU Vienna for providing free access to the OPALS software for the data processing (Pfeifer et al., 2014).

References

Ancey, C., 2020. Bedload transport: a walk between randomness and determinism. Part 2. Challenges and prospects. *Journal of hydraulic research*, 58(1), 18–33.

Buffington, J., Montgomery, D., 2013. Geomorphic classification of rivers. *In: Shroder, J.; Wohl, E., ed. Treatise on Geomorphology; Fluvial Geomorphology, Vol. 9. San Diego, CA: Academic Press. p. 730-767.*, 730–767.

Dietrich, J. T., 2017. Bathymetric Structure-from-Motion: extracting shallow stream bathymetry from multi-view stereo photogrammetry. *Earth Surface Processes and Landforms*, 42(2), 355-364.

Ferguson, R. I., Hardy, R. J., Hodge, R. A., Houseago, R. C., Yager, E. M., Yamasaki, T. N., 2024. Predicting flow resistance in rough-bed rivers from topographic roughness: Review and open questions. *Earth Surface Processes and Landforms*, 49(15), 4888-4907.

Frizzle, C., Trudel, M., Daniel, S., Pruneau, A., Noman, J., 2024. LiDAR topo-bathymetry for riverbed elevation assessment: A review of approaches and performance for hydrodynamic modelling of flood plains. *Earth Surface Processes and Landforms*, 49(9), 2585–2600.

Kinzel, P., Legleiter, C., Grams, P., 2021. Field evaluation of a compact, polarizing topo-bathymetric lidar across a range of river conditions. *River research and applications*, 37(4), 531–543.

Lague, D., Feldmann, B., 2020. Topo-bathymetric airborne LiDAR for fluvial-geomorphology analysis. *Developments in Earth Surface Processes*, 23, Elsevier, 25–54.

Legleiter, C. J., Overstreet, B. T., Glennie, C. L., Pan, Z., Fernandez-Diaz, J. C., Singhania, A., 2016. Evaluating the capabilities of the CASI hyperspectral imaging system and Aquarius bathymetric LiDAR for measuring channel morphology in two distinct river environments. *Earth Surface Processes and Landforms*, 41(3), 344-363.

Mandlburger, G., 2022. A review of active and passive optical methods in hydrography. *The International Hydrographic Review*, 8–52.

Mandlburger, G., Pfennigbauer, M., Schwarz, R., Flöry, S., Nussbaumer, L., 2020a. Concept and Performance Evaluation of a Novel UAV-Borne Topo-Bathymetric LiDAR Sensor. *Remote sensing*, 12(6), 986.

Mandlburger, G., Pfennigbauer, M., Schwarz, R., Pöppl, F., 2023. A decade of progress in topo-bathymetric laser scanning exemplified by the Pielach river dataset. *ISPRS Annals of the Photogrammetry, Remote Sensing and Spatial Information Sciences*, X-1/W1-2023, 1123–1130.

Mandlburger, G., Weiß, R., Artz, T., 2020b. Mapping of water surface levels and slopes with single photon LiDAR - A case study of the river Rhine. *The International Archives of the Photogrammetry, Remote Sensing and Spatial Information Sciences*, XLIII-B1-2020, 57–64.

Pfeifer, N., Mandlburger, G., Otepka, J., Karel, W., 2014. OPALS – A framework for Airborne Laser Scanning data analysis. *Computers, Environment and Urban Systems*, 45, 125-136.

Pfennigbauer, M., Wolf, C., Weinkopf, J., Ullrich, A., 2014. Online waveform processing for demanding target situations. M. D. Turner, G. W. Kamerman, L. M. W. Thomas, E. J. Spillar (eds), *Laser Radar Technology and Applications XIX; and Atmospheric Propagation XI*, 9080, International Society for Optics and Photonics, SPIE, 90800J.

Schwarz, R., Mandlburger, G., Pfennigbauer, M., Pfeifer, N., 2019. Design and evaluation of a full-wave surface and bottom-detection algorithm for LiDAR bathymetry of very shallow waters. *ISPRS Journal of Photogrammetry and Remote Sensing*, 150, 1-10.

Stammberger, V., Jacobs, B., Krautblatter, M., 2024. Hyperconcentrated flows shape bedrock channels. *Communications Earth Environment*, 5(1), 184.

Wang, D., Xing, S., He, Y., Yu, J., Xu, Q., Li, P., 2022. Evaluation of a New Lightweight UAV-Borne Topo-Bathymetric LiDAR for Shallow Water Bathymetry and Object Detection. *Sensors*, 22(4).

Wohl, E., 2013. *Mountain rivers revisited*. John Wiley & Sons.